HAL
open science

# Seasonal variability of the Equatorial Undercurrent at 10°W as inferred from recent in situ observations

Nicolas N. Kolodziejczyk, Bernard Bourlès, Frédéric Marin, Jacques Grelet, Rémy Chuchla

## To cite this version:

Nicolas N. Kolodziejczyk, Bernard Bourlès, Frédéric Marin, Jacques Grelet, Rémy Chuchla. Seasonal variability of the Equatorial Undercurrent at 10°W as inferred from recent in situ observations. Journal of Geophysical Research. Oceans, 2009, 114, pp.C06014. 10.1029/2008JC004976 . hal-00406930

**HAL Id: hal-00406930**

**https://hal.science/hal-00406930v1**

Submitted on 17 Jun 2014

**HAL** is a multi-disciplinary open access archive for the deposit and dissemination of scientific research documents, whether they are published or not. The documents may come from teaching and research institutions in France or abroad, or from public or private research centers.

L'archive ouverte pluridisciplinaire **HAL**, est destinée au dépôt et à la diffusion de documents scientifiques de niveau recherche, publiés ou non, émanant des établissements d'enseignement et de recherche français ou étrangers, des laboratoires publics ou privés.

# Seasonal variability of the Equatorial Undercurrent at 10°W as inferred from recent in situ observations

N. Kolodziejczyk,[1,2] B. Bourlès,[1,3] F. Marin,[1,4] J. Grelet,[5] and R. Chuchla[1,4]

Received 18 June 2008; revised 12 March 2009; accepted 6 April 2009; published 16 June 2009.

[1] Eighteen cross-equatorial shipboard current profiling sections along 10°W with conductivity-temperature-depth measurements taken between 1997 and 2007 are used to analyze the mean meridional structure and the seasonal variability of the Equatorial Undercurrent (EUC) at 10°W. Our analysis suggests a seasonal cycle for the EUC transport at 10°W, with a well-defined annual harmonic and some indication of a semiannual component, with a first maximum in January and a second stronger maximum from June to September. The mean EUC transport at 10°W is estimated to be 12.1 Sv and, compared to earlier estimates farther in the west, at 35°W (20.9 Sv) and 26°W (13.8 Sv). The eastward flow transport exhibits a strong variability at 10°W (with a total range of transports from 7.1 Sv to more than 31.7 Sv). The seasonal amplitude of the eastward flow variability is ±8.9 Sv, from a minimum of 8.2 Sv in November to 25.9 Sv in August. The eastward flows within the thermocline are divided in two parts: a permanent part within the $\sigma_\theta$ = 24.5–26.5 isopycnal layer, with a semiannual cycle, known as the EUC, and a nonpermanent part in the deep thermocline (beneath $\sigma_\theta$ = 26.5 isopycnal), associated with a strong eastward transport (up to 15 Sv) during the boreal summer, that is not observed during the rest of the year. The current at the equator in the deep thermocline is even westward during boreal fall. The disappearance of the salinity core of the EUC during the boreal summer, associated with the upwelling of the hydrological structure at 10°W, reveals that the saline subtropical waters carried by the EUC within the thermocline no longer flow into the Gulf of Guinea during the boreal summer. Our data also show the presence of the South Equatorial Undercurrent (SEUC) at 10°W in the Gulf of Guinea with a strong latitudinal and depth variability throughout the year. The mean SEUC at 10°W is centered near 5°S and is farther south than observed at 35°W and 26°W, suggesting its poleward shift from west to east.

**Citation:** Kolodziejczyk, N., B. Bourlès, F. Marin, J. Grelet, and R. Chuchla (2009), Seasonal variability of the Equatorial Undercurrent at 10°W as inferred from recent in situ observations, *J. Geophys. Res.*, *114*, C06014, doi:10.1029/2008JC004976.

## 1. Introduction

[2] Although the ocean circulation and the Equatorial Undercurrent (EUC) are rather well described and begin to be well understood in the western and central parts of the equatorial upper Atlantic Ocean [*Schott et al.*, 1998; *Bourlès et al.*, 1999; *Stramma and Schott*, 1999; *Brandt et al.*, 2006], the EUC in the Gulf of Guinea (GG) suffers from a lack of recent observations and studies.

[3] The EUC is mostly fed in the western Equatorial Atlantic with salinity and oxygen enriched waters coming from the tropics and subtropics [*Schott et al.*, 1998; *Bourlès et al.*, 1999]. Its dominant supply is from ventilated thermocline waters advected northward from the South Atlantic, predominantly via western boundary currents and, in a lesser extent, through the basin interior [*Hazeleger et al.*, 2003; *Zhang et al.*, 2003]. The connection between the waters coming from the southern hemisphere and the EUC, through the recirculation of the North Brazil Current, the North Brazil Undercurrent and the South Equatorial Current (SEC), has already been described [*Schott et al.*, 1998; *Bourlès et al.*, 1999; *Lux et al.*, 2001]. From observations taken from 1982 to 1984, studies have suggested an eastward decrease of the EUC transport [*Hisard and Hénin*, 1987; *Gouriou and Reverdin*, 1992]. More recently, the mean transport of the EUC within the $\sigma_\theta$ = 24–26.8 isopycnal range has been estimated to be 20.9 Sv near 35°W [*Schott et al.*, 2003] and 13.8 Sv near 26°W [*Brandt et al.*, 2006], thus confirming a significant eastward weakening of the mean EUC transport.

[4] In the western and central parts of the equatorial Atlantic basin, the EUC transport exhibits a semiannual cycle with two maxima in boreal spring and fall. From analysis of a 10 year long output series from a general

[1]LEGOS, OMP-PCA, Université de Toulouse III Paul Sabatier, Toulouse, France.
[2]LEGOS, IRD, Plouzané, France.
[3]LEGOS, IRD, CRHOB, Cotonou, Benin.
[4]LEGOS, IRD, Toulouse, France.
[5]US191, IRD, Plouzané, France.

Copyright 2009 by the American Geophysical Union.
0148-0227/09/2008JC004976

**Table 1.** Summary of the 18 Available Cruises Along 10°W Section

| Cruises | Month | Year | Latitudinal Range | Vessel | CTD | SADCP (KHz) |
|---|---|---|---|---|---|---|
| PIRATA-FR1 | 9 | 1997 | 10°S–2°N | L'Antea | yes | 150 |
| PIRATA-FR3 | 1 | 1999 | 6°S–2°N | L'Antea | yes | 150 |
| EQUALANT 1999 | 8 | 1999 | 10°S–2°N | La Thalassa | yes | 150 |
| PIRATA-FR5 | 10 | 1999 | 10°S–2°N | L'Antea | yes | no |
| PIRATA-FR6 | 3 | 2000 | 6°S–2°N | Le Suroît | no | 150 |
| EQUALANT 2000 | 8 | 2000 | 6°S–2°N | La Thalassa | yes | 150 |
| PIRATA-FR8 | 11 | 2000 | 10°S–2°N | L'Atalante | yes | 75 |
| PIRATA-FR9 | 10 | 2001 | 10°S–2°N | L'Atalante | yes | 75 |
| PIRATA-FR11 | 12 | 2002 | 10°S–1.5°N | Le Suroît | yes | 150 |
| PIRATA-FR12 | 2 | 2004 | 10°S–1.5°N | L'Atalante | yes | 75 |
| CORIOLIS 2003 | 5 | 2003 | 10°S(2.5W)–10°N(17°W) | Le Beautemps-Beaupré | no | 38 |
| CORIOLIS 2004 | 8 | 2004 | 10°S(2.5W)–10°N(17°W) | Le Marion Dufresne | no | 38 |
| EGEE 1 | 6 | 2005 | 10°S–2°N | Le Suroît | yes | 150 |
| EGEE 2 | 9 | 2005 | 10°S–2°N | Le Suroît | yes | 150 |
| EGEE 3 | 6 | 2006 | 10°S–2°N | L'Atalante | yes | 75 |
| EGEE 4 | 11 | 2006 | 6°S–2°N | L'Atalante | yes | 75 |
| EGEE 5 | 6 | 2007 | 10°S–2°N | L'Antéa | yes | 75 |
| EGEE 6 | 9 | 2007 | 3°S–2°N | L'Antéa | yes | 75 |

circulation model, *Arhan et al.* [2006] suggest that two distinct mechanisms drive the EUC semiannual cycle in the western equatorial Atlantic: the spring maximum is associated with enhanced equatorial ventilation by extra-equatorial winds, while the fall maximum is induced by the intensification of the westward wind and the zonal pressure gradient (ZPG) along the equatorial band [*Katz et al.*, 1981; *Giarolla et al.*, 2005].

[5] In the eastern part of the basin, the EUC seasonal variability has not been studied yet in detail from in situ observations. Presently, the termination of the EUC is poorly documented, and sparse studies suggest a strong variability of the EUC in the GG [*Voituriez*, 1983; *Hisard and Hénin*, 1987; *Wacongne and Piton*, 1992; *Bourlès et al.*, 2002]. In this region, numerical models [e.g., *Philander and Pacanowski*, 1986] indicate that the semiannual fluctuations dominate the EUC variability. At 10°W and 3°E, *Arhan et al.* [2006] suggest also two maxima of the EUC transport. The first maximum occurs in boreal fall, like in the west, but the second maximum occurs in boreal winter, and not in boreal spring as in the western basin.

[6] In this study we present an original set of observations obtained along 10°W in the equatorial region which allows a better description and understanding of the circulation variability at this particular longitude, i.e., at the entrance of the GG. From horizontal current measurements and hydrological sections collected at different periods of the year from 1997 to 2007, we present the mean structure of the EUC and then describe the EUC seasonal cycle at 10°W, along with a short description of the South Equatorial Undercurrent (SEUC).

## 2. Data and Processing

### 2.1. Cruises Data

[7] The data used in this study were collected between 1997 and 2007 during several cruises carried out in the framework of different programs, namely the Prediction and Research moored Array in the Tropical Atlantic program (the former Pilot Research moored Array in the Tropical Atlantic program (PIRATA) [*Servain et al.*, 1998; *Bourlès et al.*, 2008]), the EQUALANT program [*Bourlès et al.*, 2002], the EGEE program (as part of the African Monsoon Multidisciplinary Analysis program AMMA [*Redelsperger et al.*, 2006]), and also from other French cruises, carried out in the framework of the French CORIOLIS project (see http://www.CORIOLIS.eu.org/). All these cruises are summarized in Table 1, and a total of 18 sections are thus available at the longitude 10°W (Figure 1).

[8] During 17 cruises, ship-mounted acoustic Doppler current profiler (SADCP) observations were collected continuously along the track lines, providing the two horizontal components of the current velocity. The vertical resolution, surface cut off (generally the top 20 m) and depth penetration of the ADCP current measurements vary accordingly with the SADCP instrument, i.e., with the frequency of the SADCP used (see Table 1). SADCP measurements cover the depth range from 20 m down to about 250 m, depending upon the cruise. Such a vertical extent allows a full description of the EUC core, but generally the SEUC cannot be fully described. During each cruise, absolute referencing was provided by Global Positioning System (GPS) navigation. All the SADCP data were first hourly averaged, then linearly interpolated on a regular grid with a resolution of 0.1° in latitude and 1 m in depth. The accuracy of the horizontal current velocity (3 cm $s^{-1}$) has been estimated through the mean standard deviation of these hourly averaged SADCP data, following *Bourlès et al.* [2002]. These data were used to estimate the transports of the EUC and the resolved part of the SEUC. Eastward transports have been calculated within contours of positive zonal velocities. They do not include the velocities above the ADCP cutoff depth, thus potentially underestimating near-surface eastward transports.

[9] During 15 cruises (see Table 1), conductivity-temperature-depth (CTD) measurements were also taken with SeaBird probes. Water samples were done for conductivity sensors calibration during the EQUALANT and EGEE cruises, and during every PIRATA cruises carried out from 2004. The CTD sensors were systematically calibrated before and after the cruises and the accuracy is around ±0.003°C for the temperature and ±0.003 for the salinity. The horizontal resolution of the CTD profiles along 10°W is generally of 1/2° of latitude, but is 1/3° between 1°S and 1°N during the EQUALANT and EGEE cruises and 1° during every PIRATA cruises carried out before 2004.

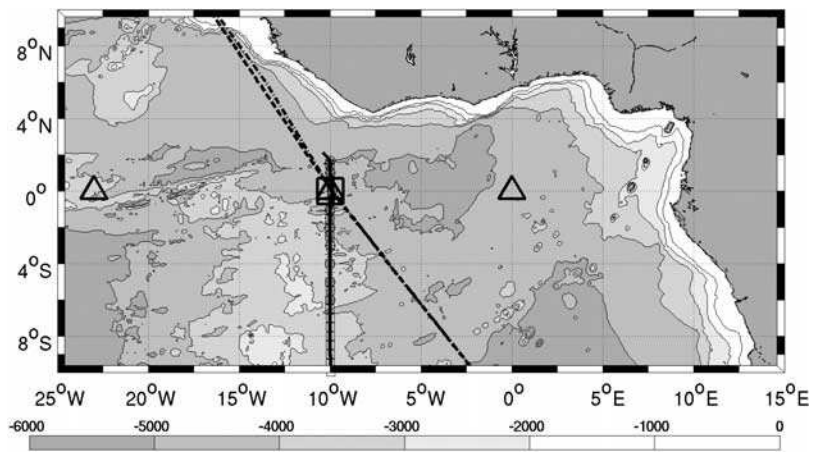


**Figure 1.** Track lines of the 18 cruises along 10°W in the Gulf of Guinea carried out between 1997 and 2007 and used in this study. CORIOLIS 2003 and 2004 (dash-dotted line and dashed line, respectively) cross the equator at 10°W. EQUALANT, PIRATA, and EGEE cruises are shown by the solid line along the 10°W section, and CTD stations are shown by stars, squares, and circles. The triangles localize the PIRATA moorings providing temperature and wind measurements. The large square at 0°N–10°W localizes the current meter mooring providing zonal velocity data between 2003 and 2005. Gray shading is the bathymetry in meters.

### 2.2. Moored ADCP Data

[10] High time resolution currents are available at 10°W–0°N from the surface down to about 290m depth thanks to an ADCP mooring deployed without any interruption from May 2003 to June 2005, in the framework of the French component of the PIRATA program [*Bunge et al.*, 2007].

### 2.3. Climatological Data From ARIVO

[11] Monthly climatological data are used to estimate the zonal pressure gradient (ZPG) at 10°W along the equator. We use the ARIVO (Analyse, Reconstruction et Indicateurs de la Variabilité Océanique) climatology that is constructed from Levitus climatology with addition of recent ARGO float measurements, cruises data and PIRATA moorings measurements [*Gaillard et al.*, 2009]. The ARIVO climatology provides temperature-salinity profiles with a vertical resolution of 5 m. XBT data are removed from the climatology because of the biases in the depth estimation of the measurements. To estimate the ZPG, the monthly density profiles at 23°W, 10°W and 0°E are first computed from the ARIVO temperature-salinity monthly climatological profiles at these longitudes, using the equation of state defined in the work by *Millero et al.* [1980] and *Fofonoff and Millard* [1983]. We choose these longitudes because of the presence of the PIRATA moorings that minimizes the a priori errors (K. von Schuckmann, personal communication, 2008). The ZPG is then calculated following the equation:

$$ZPG_i(10^\circ W) = g\sum_{k=0}^{i}\left\{\frac{\delta_1(\rho_k(0^\circ E)-\rho_k(10^\circ W))}{X_{0^\circ E}-X_{10^\circ W}} + \frac{\delta_2(\rho_k(10^\circ W)-\rho_k(23^\circ W))}{X_{10^\circ W}-X_{23^\circ W}}\right\}\Delta z, \quad (1)$$

which corresponds to the weighted average of the ZPG calculated between 23°W and 10°W, and between 10°W and 0°E, with $X$ the longitude, $\rho$ is the density, and g = 9.8 m s$^{-1}$. $\delta_1$ = 0.5652 and $\delta_2$ = 0.4348 represent weights, calculated from the distances between the two pairs of longitudes in order to estimate the ZPG exactly at 10°W. The ZPG is integrated upward from 500 m depth ($k$ = 0) to the depth $z$ (index $i$), with a vertical spacing $\Delta z$ = 1 m. The choice of 500 m depth as the level of reference may introduce errors into our ZPG estimate. To assess the amplitude of these errors, we have compared the seasonal anomalies of the surface ZPG estimated from climatological data and from the gridded altimetric product of Sea Level Anomalies (SLA) provided by AVISO and combining all available altimetry satellites (see http://www.aviso.oceanob.com/). The two seasonal cycles are well correlated at about 81% (not shown). The amplitude of the surface ZPG estimated from ARIVO is not larger than 20% than the one deduced from AVISO between January and October. The largest difference is observed during boreal fall. This good comparison between the two estimates gives us confidence that the ZPG calculated from ARIVO is realistic.

### 2.4. PIRATA Mooring Temperature and Wind Data

[12] In the framework of the PIRATA program, meteo-oceanic moorings are maintained since 1997 along the equator in the Atlantic, namely at 35°W, 23°W, 10°W and 0°E. These moorings provide high-resolution (daily) time series of temperature measurements at 11 depth levels from the surface down to 500 m depth, with a 20 m resolution from the surface down to 140m depth. Wind measurements are at an altitude of 4 m above the sea surface (see http://www.brest.ird.fr/PIRATA/ for details on the PIRATA data sets). From September 1997 to January 2008 time series, we calculated a mean composite seasonal cycle of the thermal structure for each PIRATA buoy location. Because of some gaps in the data sets (refer to the PIRATA web site for details), only 8.8, 7.4, 3.5 and 4.9 years of data were available at 35°W, 23°W, 10°W and 0°E, respectively, for the wind. And 6.4 years of data were available at 10°W for

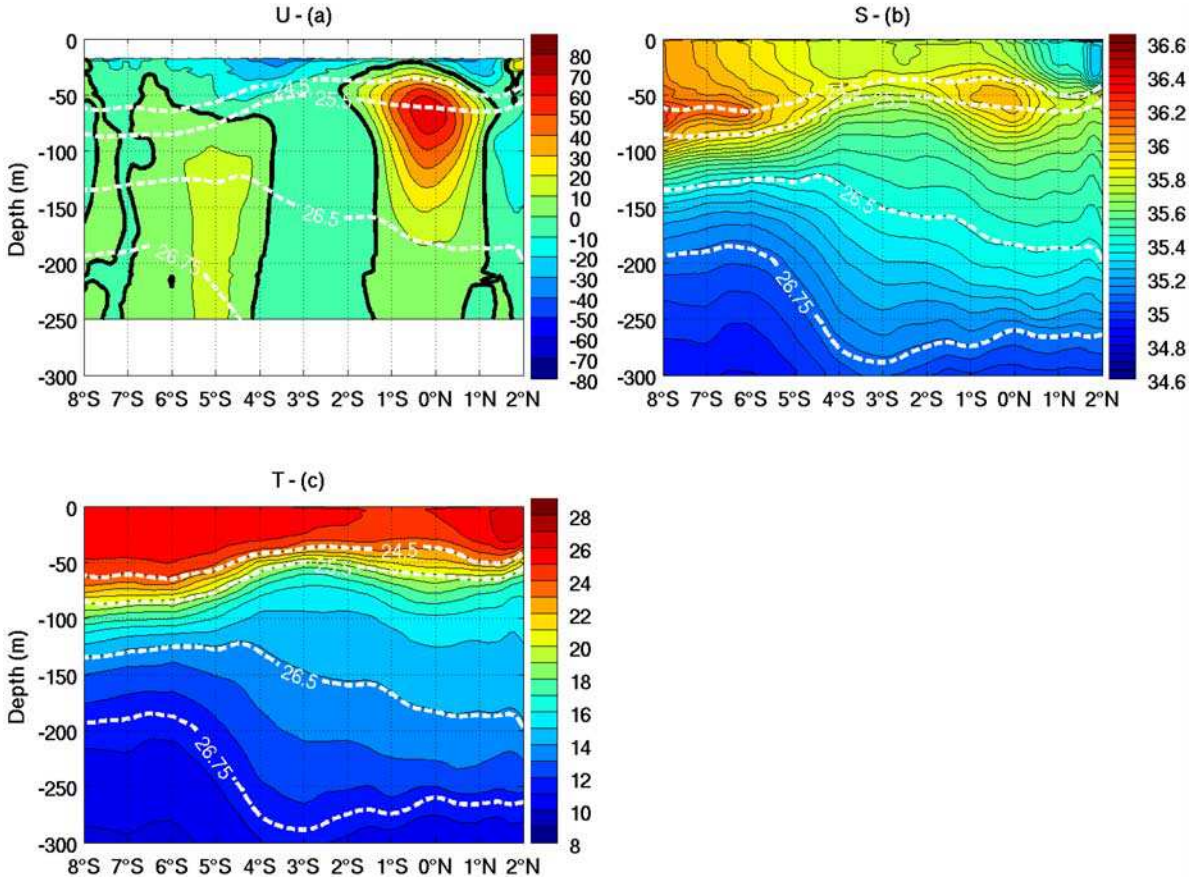


**Figure 2.** Mean meridional section at 10°W: (a) zonal velocity (cm $s^{-1}$), (b) salinity, and (c) temperature (°C). The white curves are the isopycnal contours, from surface to depth: $\sigma_\theta = 24.5$, $\sigma_\theta = 25.5$, $\sigma_\theta = 26.5$, and $\sigma_\theta = 26.75$.

subsurface temperature. The most complete time series obtained over one a full year for all three moorings were obtained in 2003, 2006 and 2007, thus the cycle may be weakly biased. The data have been smoothed with a 50-day running mean filter in order to filter out the intraseasonal variability.

## 3. Mean Sections at 10°W

[13] In order to provide a mean view of the zonal circulation at the entrance of the GG, we have computed mean sections of zonal velocity, temperature and salinity from our 17 SADCP and 15 CTD available sections. These mean sections are presented in Figure 2 and can be directly compared with mean equatorial sections previously presented at 35°W by *Schott et al.* [2003] and around 26°W by *Brandt et al.* [2006]. As summarized in Table 2, 3 cruises were carried out in boreal winter (i.e., from December to February), 2 in spring (March to May), 6 in summer (June to August) and 7 in fall (September to November). The SADCP and CTD sections are mainly distributed in summer and fall, which may introduce some seasonal bias in these mean sections. Most cruises (except in September 2007) cover the latitudinal range between 6°S and 1.5°N. Part of the 10°W section comprised between 10°S and 6°S was not sampled during 5 cruises (Table 1), thus under-sampling zonal currents south of 6°S. Note that no CTD profile is available in spring, so the mean hydrological structure does not take into account the spring conditions. In order to facilitate the description, and the comparisons with other studies of mean currents in the Equatorial Atlantic, we define the mean thermocline depth as the depth of the $\sigma_\theta = 25.5$ isopycnal, which corresponds to the location of the maximum vertical gradient of temperature, and decompose the water column into 4 isopycnal layers: the surface layer ($\sigma_\theta$ above 24.5), the upper thermocline ($\sigma_\theta$ between 24.5 and 25.5), the lower thermocline ($\sigma_\theta$ between 25.5 and 26.5) and the deep thermocline ($\sigma_\theta$ below 26.5).

### 3.1. Mean Flow at 10°W

[14] The EUC is characterized by eastward zonal velocities that are observed mostly between the $\sigma_\theta = 24.5$ and 26.5 isopycnals, i.e., between 25 m and 180 m depth (Figure 2a). It is bordered by the central and northern branches of the westward South Equatorial Current (SEC) [*Stramma and Schott*, 1999]. The mean EUC velocity core is found at 0.2°S with a maximum eastward velocity up to 69 cm $s^{-1}$, and centered around 64 m depth along the isopycnal $\sigma_\theta = 25.5$ (Table 3). The EUC appears to have a larger extent in the southern hemisphere, as far as 2°S around 50 m depth.

[15] The EUC total transport estimated from the mean section is 12.1 Sv (Table 2). This value has to be compared with the 20.9 Sv found by *Schott et al.* [2003] at 35°W, and

**Table 2.** EUC Total Transport for Each Cruise and Transport in Each Isopycnal Layer Defined in the Text

| | Total Transport (Sv) | Isopycnal Layer[a] | | | |
|---|---|---|---|---|---|
| | | Surface | Upper | Lower | Deep |
| Date | | | | | |
| Jan 1999 | 13.4 | 2.4 | 2.1 | 7.9 | 0.9 |
| Feb 2004 | 14.8[b] | 2.2 | 3.2 | 9.4 | 0.1 |
| Mar 2000 | 7.4 | .. | .. | .. | .. |
| May 2003 | 12.7[b] | .. | .. | .. | .. |
| Jun 2005 | 20.2[b] | 0 | 0.3 | 14.3 | 5.7[b] |
| Jun 2006 | 24.4 | 0.5 | 1.1 | 13.6 | 9.2 |
| Jun 2007 | 9.3 | 0.2 | 0.7 | 7.6 | 0.8 |
| Aug 1999 | 31.7[b] | 0 | 1.3 | 15.1 | 15.3[b] |
| Aug 2000 | 20.0 | 0 | 1.9 | 10.7 | 7.2 |
| Aug 2004 | 24.6 | .. | .. | .. | .. |
| Sep 2007 | 27.3 | 7.1 | 5.4 | 11.7 | 3.1 |
| Sep 2005 | 17.4 | 3.3 | 4.6 | 7.5 | 2.0 |
| Sep 1997 | 11.2 | 1.0 | 4.0 | 6.2 | 0 |
| Oct 2001 | 7.8 | 0.7 | 1.5 | 5.2 | 0.4 |
| Nov 2006 | 9.6 | 0.8 | 1.2 | 7.8 | 0.2 |
| Nov 2000 | 7.1 | 0 | 0.7 | 6.3 | 0 |
| Dec 2002 | 11.2[b] | 0.9 | 2.2 | 8.0 | 0.2 |
| Mean of transports | 15.9 ± 7.6[b] | 1.3 ± 1.9 | 2.2 ± 1.6 | 9.3 ± 3.2 | 3.1 ± 4.6[b] |
| Averaged section | 12.1 ± 1.9 | 0.4 ± 0.2 | 2.5 ± 0.2 | 8.3 ± 0.8 | 0.9 ± 0.8[b] |

[a]Surface, $\sigma_\theta < 24.5$; upper layer, $24.5 < \sigma_\theta < 25.5$; lower layer, $25.5 < \sigma_\theta < 26.5$; deep layer, $\sigma_\theta > 26.5$.
[b]The transport is underestimated.

to the 20.0 Sv and 13.8 Sv obtained at 35°W and around 26°W, respectively, by *Brandt et al.* [2006]. These results suggest that, while the EUC transport significantly decreases from 35°W to 26°W and loses about 6 Sv, it decreases only modestly farther east, losing 1.7 Sv between 26°W and 10°W. From the 12.1 Sv EUC total transport, 0.4 Sv occurs in the surface layer, i.e., above $\sigma_\theta = 24.5$ (as previously defined by *Schott et al.* [2003] and *Brandt et al.* [2006]), and 11.7 Sv in the thermocline as follows: 2.5 Sv in the upper thermocline, 8.3 Sv in the lower thermocline layer, and 0.9 Sv in the deep thermocline above 250 m depth (Table 2). *Brandt et al.* [2006] found at 26°W an EUC transport of 3.1 Sv above $\sigma_\theta = 24.5$ and 10.7 Sv below. Thus, between 26°W and 10°W, the EUC loses about 2.7 Sv above $\sigma_\theta = 24.5$ but gains 1.0 Sv below. A remarkable result is that the largest part (about 70%) of the EUC transport at 10°W occurs in the lower thermocline, i.e., below the EUC core which is located along the isopycnal $\sigma_\theta = 25.5$. This can be explained by the presence of stronger eastward velocities below 100 m at 10°W than at 26°W, corresponding to a larger vertical extension of the EUC at that longitude.

[16] The standard error of the mean EUC transport estimated from the mean section at 10°W was evaluated from the standard error of EUC transports calculated for each individual sections under the assumption of independent realizations, as in the work by *Brandt et al.* [2006]. The error of the mean EUC transport is thus determined to be 1.9 Sv, and is similar to the estimates reported by *Brandt et al.* [2006] at 35°W (1.6 Sv) and 23°W (1.7 Sv). These errors are comparable to the EUC transport decrease between 23°W and 10°W (1.7 Sv), thus moderating the conclusion of an eastward decrease of the EUC transport.

[17] If now the mean eastward flow transport is estimated through the average of the eastward flow transports for each individual section, it becomes 15.9 Sv. The large standard deviation (7.6 Sv) of the individual transports is the signature of a strong variability of the eastward flow transport at 10°W, ranging from 7.1 Sv in November 2000 to a maximum value of 31.7 Sv in August 1999 (Table 2). This result shows that the average of the individual transports is stronger (by 3.8 Sv) than the transport estimated from the mean zonal velocities. This indicates a large variability in the vertical distribution of the eastward flows. This transport increase occurs in the surface layer (0.9 Sv) and in the lower part of the thermocline (1.0 Sv in the lower thermocline and 2.2 Sv in the deep thermocline), while the upper thermocline contribution is small and negative (−0.3 Sv).

**Table 3.** Main Characteristics Observed for the EUC During Each Cruise[a]

| | Vmax (cm s$^{-1}$) | Z (m) | Latitude (deg) | Width (km) | Thermocline Thickness (m) | Thermocline Depth (m) |
|---|---|---|---|---|---|---|
| Date | | | | | | |
| Jan 1999 | 88 ± 3 | 57 | −0.4 | 444 | 113 | 59 |
| Feb 2004 | 101 ± 4 | 61 | −0.6 | >312 | 146 | 61 |
| Mar 2000 | 83 ± 3 | 49 | −0.1 | 522 | .. | .. |
| May 2003 | 94 ± 4 | 73 | −0.9 | 301 | .. | .. |
| Jun 2005 | 95 ± 2 | 52 | −0.2 | 245 | 169 | 29 |
| Jun 2006 | 89 ± 2 | 45 | −0.4 | 289 | 148 | 47 |
| Jun 2007 | 60 ± 3 | 60 | −0.1 | 178 | 185 | 46 |
| Aug 1999 | 89 ± 4 | 55 | −0.3 | 356 | 144 | 41 |
| Aug 2000 | 85 ± 2 | 64 | 0.3 | 356 | 175 | 42 |
| Aug 2004 | 93 ± 6 | 63 | −0.1 | 189 | .. | .. |
| Sep 2007 | 108 ± 3 | 91 | −0.1 | 467 | 109 | 94 |
| Sep 2005 | 92 ± 1 | 79 | −0.7 | 388 | 164 | 83 |
| Sep 1997 | 57 ± 4 | 73 | −0.2 | 367 | 177 | 73 |
| Oct 2001 | 61 ± 2 | 76 | −0.1 | 367 | 160 | 73 |
| Nov 2006 | 86 ± 3 | 75 | 0.2 | 322 | 148 | 65 |
| Nov 2000 | 74 ± 4 | 77 | 0.6 | 278 | 159 | 57 |
| Dec 2002 | 90 ± 3 | 67 | 0.2 | >267 | 132 | 62 |
| Means | 84 ± 15 | 69 ± 13 | −0.2 ± 0.4 | 338 ± 97 | 152 ± 23 | 59 ± 23 |
| Averaged section | 69 ± 5 | 64 | −0.2 | 367 | 145 | 61 |

[a]First column, month of the campaign along with means and averaged section; second column, maximum velocity of the EUC; third column, depth of the EUC core; fourth column, latitude of the EUC core; fifth column, width of the EUC; sixth column, thermocline thickness; and seventh column, thermocline depth. The width is taken at the depth of the maximum velocity between zero isotachs. The thermocline thickness is taken at the latitude of the core within $\sigma_\theta = 24.5–26.5$. The thermocline depth is the depth of $\sigma_\theta = 25.5$.

[18] The two estimates of the mean EUC transport encompass also the mean transport estimated at 23°W (13.8 Sv) by *Brandt et al.* [2006]. The eastward decrease of the EUC transport can thus not been evidenced unambiguously from our analysis. Which one of the transport estimates is the most representative of the EUC mean transport? Figure 2a and Table 2 show that the eastward transports in the surface and the deep layers (less than 1 Sv in both layers) are minimized when velocities are averaged to provide the mean section. This suggests that a westward flow may compensate the eastward flows, i.e., that the eastward flows are nonpermanent in these layers during the year. So, the average of the individual transports, taking into account only the eastward flows, is likely to overestimate the mean eastward transport in these layers and thus the estimated mean EUC transport at 10°W. Consequently, the EUC transport deduced from the mean section is more representative of the EUC mean transport, and the nonpermanent part of the eastward flow observed in the surface and deep layers should not be considered as part of the EUC.

[19] Another eastward current is observed centered at 5°S below 100 m with zonal velocities exceeding 10 cm $s^{-1}$. It corresponds to the SEUC, also observed at 35°W and 26°W [*Schott et al.*, 2003; *Brandt et al.*, 2006]. The eastward velocities associated with the SEUC are found between 4°S and 7°S, revealing a large latitudinal extent for this mean current at that longitude. This current has a strong geostrophic signature in the hydrological structure with an equatorward deepening of the 26.75 isopycnal and equatorward shallowing of the $\sigma_\theta = 25.5$ isopycnal, at the origin of the equatorial pycnostad north of 5°S. The transport of the mean SEUC is estimated to be 4.3 Sv. Note that this transport (1) must be underestimated because of the cutoff depth of the SADCP, that does not allow to capture the whole vertical extent of this current, and (2) is calculated from 16 sections. This transport is of the same order of magnitude as the 4.8 Sv estimated at 26°W by *Brandt et al.* [2006, Figure 1] within the $\sigma_\theta = 24.5–26.8$ isopycnal range. However the mean velocities are weaker at 10°W than at 26°W or 35°W, and the mean latitudinal position of the SEUC core (5°S) is further from the equator than at 26°W (4°S) and 35°W (3°S). The SEUC is present during each cruise at 10°W, indicating that it permanently penetrates into the GG, keeping its transport nearly constant and shifting poleward from west to east.

### 3.2. Mean Salinity and Temperature Section at 10°W

[20] Salinity and temperature mean sections shown in Figures 2b and 2c illustrate the mean water mass distribution along 10°W. The salient feature in the vertical salinity distribution is the presence of two distinct maxima in the upper thermocline: the first salinity core (>36.0) is observed around the equator extending between 1.5°S and 1°N and takes place in the upper core of the EUC. The second salinity maximum (>36.0) is found south of 4°S, extending up to the surface south of 5°S, and is the signature of subtropical waters. Even though the 24.5 isopycnal coincides with relative salinity maximum from 8°S to 2°N, the existence of two distinct maxima indicates that there is no direct meridional flow along 10°W from the south toward the equator that could feed the EUC with subtropical waters. The connection between the subtropical thermocline waters and the EUC water mass must then occur west of 10°W through more western pathways, in the west or the center of the basin [*Hazeleger et al.*, 2003; *Zhang et al.*, 2003]. In the lower thermocline, salinity decreases with depth.

[21] Near the equator, the EUC core is characterized by a vertical broadening of the thermal structure between the 16°C and 24°C isotherms (Figure 2c). Between 6°S and 3°S, below the 16°C isotherm, the thermal structure deepens toward the equator and corresponds to the geostrophic signature of the SEUC. It is the southward limit of a region with weak vertical gradient of temperature, known as the 14°C thermostad [*Tsuchiya*, 1986]. There is a strong similarity in the vertical distributions of temperature and zonal velocity at the equator: the strongest vertical gradients of temperature between 50 m and 100 m coincide with the strongest vertical gradients of the zonal velocity, above the EUC core, whereas the lower part of the EUC is characterized by lower vertical gradients of temperature and velocity.

[22] At the surface, salinity distribution is asymmetric with respect to the equator, with low-salinity surface waters north of the equator that contrast with the subtropical saline surface waters observed south of 5°S (Figure 2b). This low surface salinity at 10°W has been reported as mainly influenced by the negative Evaporation minus Precipitations budget in the eastern Atlantic [*Dessier and Donguy*, 1994]. The temperature relative minimum observed at about 1°S (<25°C) is the signature of the boreal summer cold tongue due to the equatorial upwelling, which separates warm surface waters (>25°C) present in both hemispheres (Figure 2c).

## 4. Seasonal Cycle of the EUC at 10°W

### 4.1. Seasonal Cycle of the EUC Transport

[23] Figure 3a presents the total eastward transports associated with the EUC at 10°W, and the respective contributions of the four layers defined above, obtained from our 17 cruises (Figures 3b, 3c, and 3d; see also Table 2). We observe that the eastward total transport (squares in Figure 3a) presents a first relative maximum in January–February (up to 14.8 ± 1.4 Sv), followed by a rapid weakening leading to a minimum in March (down to 7.4 ± 0.8 Sv, though only sampled by one section), then strongly increases to be maximum in August (up to 31.7 ± 3.2 Sv), and finally decreases from September to reach a second relative minimum in October–November (down to 7.1 ± 0.9 Sv). We fit the total eastward transport (Figure 3a) and the transport within the thermocline (i.e., $24.5 < \sigma_\theta < 26.5$ (Figure 3b)) with a least squares regression on annual and semiannual harmonics. The harmonic fitting indicates a seasonal variability with an amplitude of 8.9 Sv (Figure 3a; 6.2 Sv and 4.8 Sv for the annual and semiannual harmonics, respectively, computed separately), suggesting a predominance of the annual harmonics over the semiannual harmonics. The EUC transport within the $\sigma_\theta = 24.5–26.5$ also fits with a seasonal cycle in phase with the total transport (Figure 3b), but with a smaller amplitude (4.7 Sv) and with comparable contributions of the annual (2.6 Sv) and semiannual (2.7 Sv) harmonics. Uncertainties of these estimates have been computed as the standard deviations of the data to the fitted harmonics. Error estimates on the

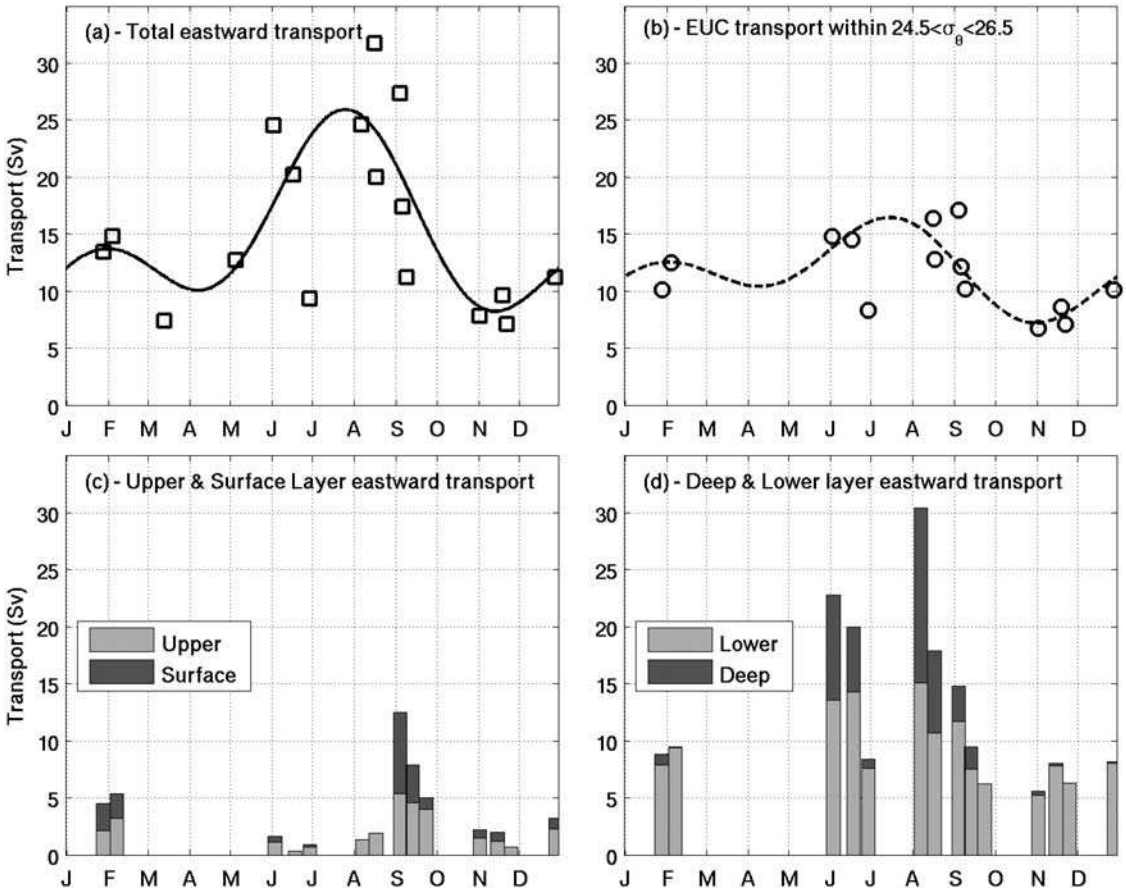


**Figure 3.** Repartition of the EUC transports for the different density layers during the year from SADCP data collected during 17 cruises: (a) total eastward transport (squares), (b) eastward transport within the $\sigma_\theta$ = 24.5–26.5 layer (circles), (c) eastward transports in the surface layer (dark gray) and thermocline upper layer (light gray), and (d) eastward transports in the lower (light gray) and deep (dark gray) thermocline. See the text for the definition of the layers. Fits to annual and semiannual harmonics are indicated in Figure 3a (solid curve) and Figure 3b (dashed curve). Only SADCP in the presence of CTD measurements are indicated in Figures 3b–3d.

amplitude of the seasonal cycle are then 5.8 Sv for the total transport and 2.6 Sv for the transport within the thermocline, indicating a large deviation of the data from the fitted curves.

[24] Note that the lack of CTD observation during boreal spring (Table 1 and Figure 3b) does not allow to confirm the minimum of transport within this layer during this period of the year. But the minima in the total transport in March and May (Figure 3a and Table 2) compared to the seasonal cycle of the transport within $\sigma_\theta$ = 24.5–26.5, suggest that the transport is also minimum within this layer in boreal spring. Thus, in spite of interannual or intraseasonal events that may significantly alter the seasonal variability, the observations analyzed here tend to suggest the existence of a semiannual cycle and confirm the strong boreal summer maximum for the EUC transport at 10°W, as earlier suggested from realistic numerical simulations [*Philander and Pacanowski*, 1986; *Arhan et al.*, 2006].

[25] The transports in the surface layer and in the upper thermocline provide only a small contribution to the seasonal cycle of the EUC transport (Figure 3c). Even weak (or null in the surface layer) most of the year, both transports exhibit however two maxima in boreal winter (January and February) and in September. The maximum contributions of these two layers to the total transport are found in February 2004 (5.5 Sv) and in September 2007 (12.5 Sv).

[26] In contrast, the transport variability in the lower thermocline is larger and exhibits a similar seasonal evolution as the total transport (Table 2 and Figure 3d), with a strong maximum in summer (up to 15.1 Sv in August 1999), a minimum in fall (down to 5.2 Sv in October 2001) and a weaker second maximum in winter (9.4 Sv in February 2004).

[27] The most noticeable feature is the presence of strong eastward transports in the deep thermocline in boreal summer, particularly in August (reaching more than 15.3 Sv in August 1999 (Table 2 and Figure 3d)), while they are rather negligible during the rest of the year. In particular, in contrast with the lower thermocline, there is no intensification of the transport in boreal winter.

[28] Thus, the seasonal variability of the EUC transport is in large part explained by the seasonal evolution of the transport in the lower and deep thermocline. Note that the strong summer maximum is concomitant with the

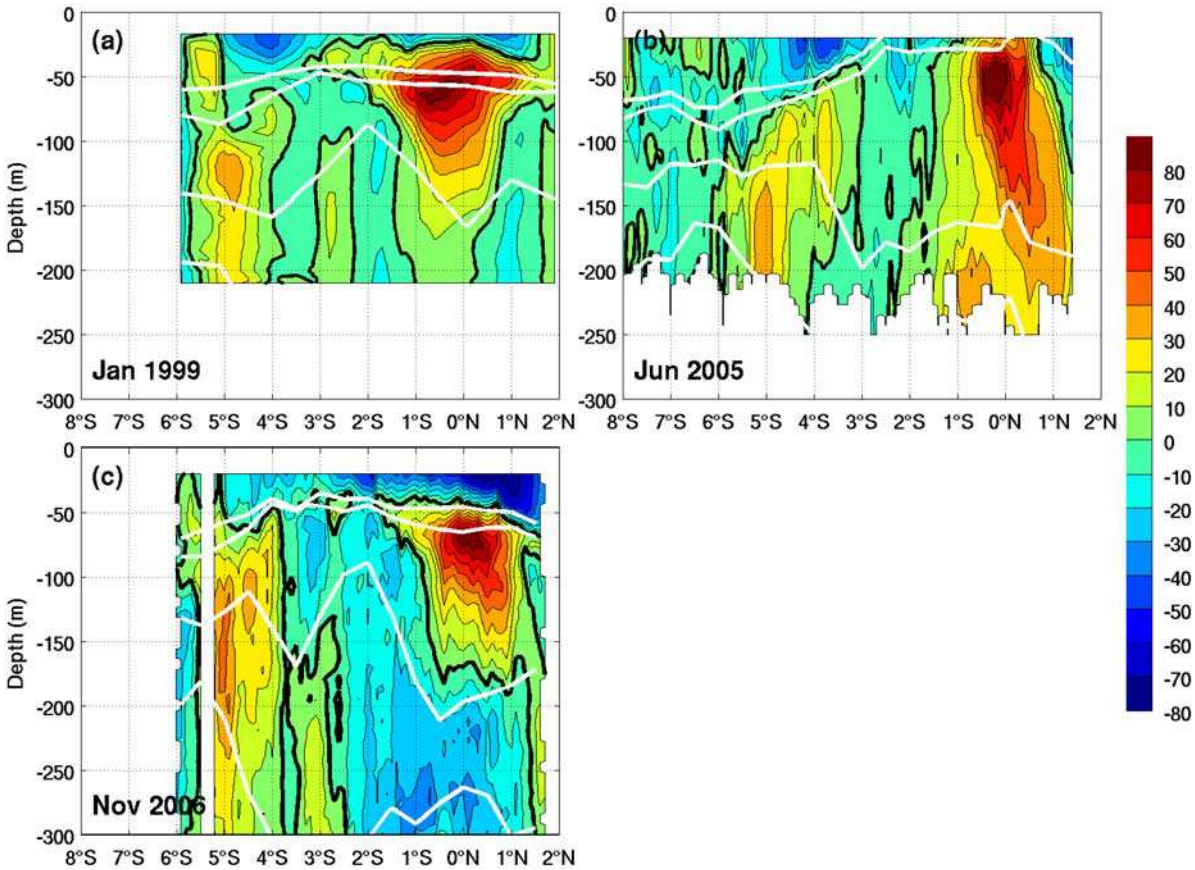


**Figure 4.** Meridional sections of zonal velocity at 10°W between 300 m depth and the surface and 8°S and 2°N (a) during PIRATA-FR3 cruise in January 1999, (b) during EGEE 1 cruise in June 2005, and (c) during EGEE 4 cruise in November 2006. Velocities are in centimeters per second. Isotach 0 is indicated by the bold line.

appearance of an intense eastward transport below $\sigma_\theta = 26.5$ that does not exist or is very weak during the other seasons.

### 4.2. Seasonal Variability in EUC Structure

#### 4.2.1. Boreal Winter Maximum

[29] During the three cruises carried out in boreal winter, i.e., from December to February, the EUC core is located around 60 m depth (from 57 m to 67 m), centered around the $\sigma_\theta$ = 25.5 isopycnal, as illustrated in Figure 4 for January 1999. Its intensity varies from 88 to 101 cm s$^{-1}$ (Table 3). The EUC also presents a large latitudinal extent, as large as 444 km in January 1999, and extends down to 200 m (Figure 4a).

[30] In boreal winter eastward velocities are observed above $\sigma_\theta$ = 24.5 (Figure 4a), explaining the January–February maximum of eastward transport in the surface layer. During this season, the trade winds weaken or even reverse in the equatorial Atlantic, thus failing to maintain the surface westward stress opposing the ZPG, and yielding the relaxation of the eastward surface flow above the EUC as shown earlier by *Hisard and Hénin* [1987].

#### 4.2.2. Boreal Summer Maximum

[31] From June to August, the EUC velocity core is observed between 45 and 64 m depth, with zonal velocities between 60 and 95 cm s$^{-1}$ according to the cruise (Table 3). The most striking feature during this period of the year is the deep extension of eastward velocities (exceeding 30 cm s$^{-1}$) below $\sigma_\theta$ = 26.5 close to the equator, as illustrated in Figure 4b for June 2005. Such a deep extension is a permanent feature for all cruises carried out in August.

[32] On the other hand, the $\sigma_\theta$ = 24.5 isopycnal outcrops at the surface and the EUC velocity core is observed entirely below $\sigma_\theta$ = 25.5 during this period (Figure 4b). The estimated eastward transport associated with the EUC is maximum during this period of the year, and the maximum transport (31.7 Sv) has been estimated in August 1999 (Table 3).

[33] In September, the EUC velocity core is observed between 73 and 91 m depth, around or below $\sigma_\theta$ = 25.5, and exhibits maximum of zonal velocity varying from 57 to 108 cm s$^{-1}$ (Table 3). The transport in the deep thermocline strongly decreases, while simultaneously the transports in the upper thermocline and surface layers are at their yearly maximum (Table 2). This explains why the total EUC transport in September has comparable values than the boreal summer ones.

#### 4.2.3. Boreal Fall Minimum

[34] In October–November the vertical structure of zonal currents near the equator is very different from the summer one (Figure 4c). While an intense EUC is still present in the lower and upper thermocline, currents are now westward above $\sigma_\theta$ = 24.5 and beneath $\sigma_\theta$ = 26.5. At the surface, this

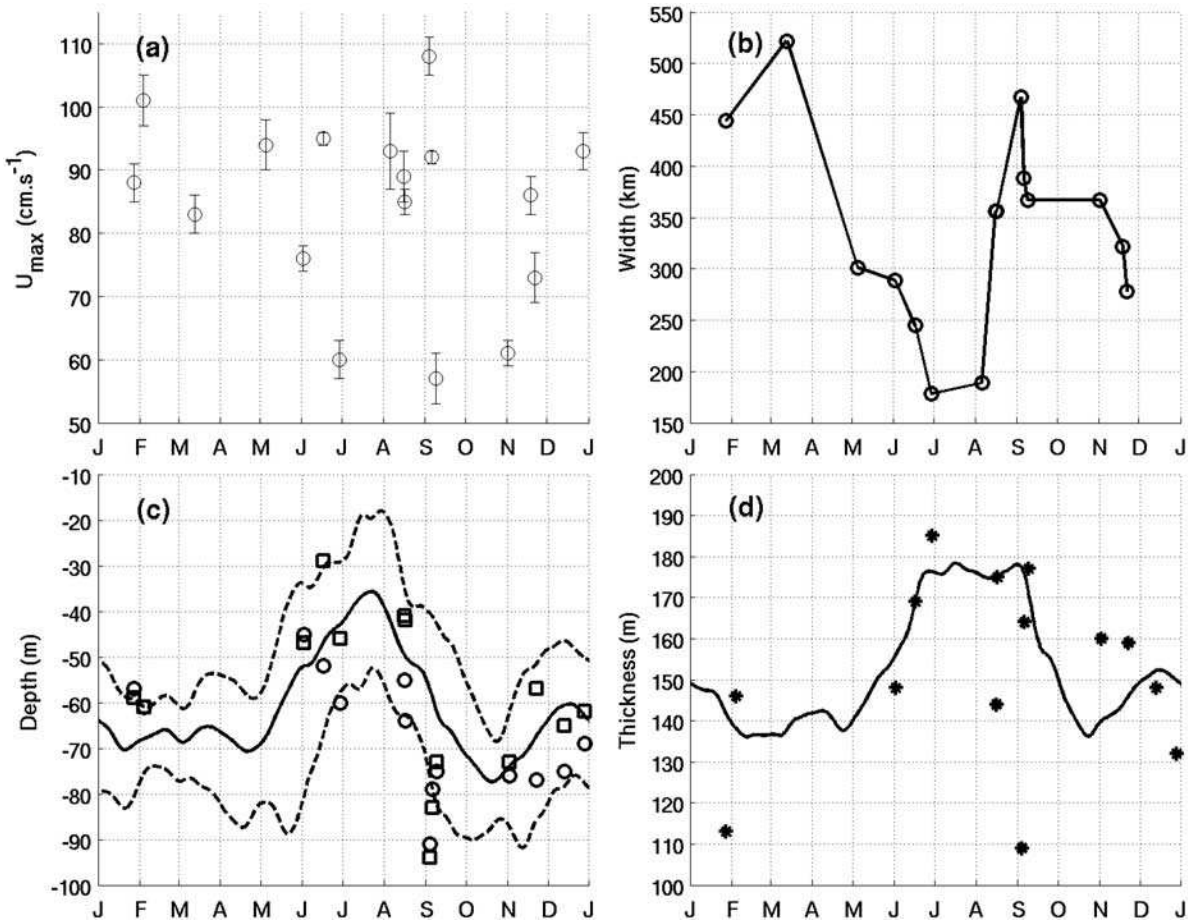


**Figure 5.** (a) Repartition of the total maximum velocity with error bars during the year with data collected during 17 cruises (m s$^{-1}$). (b) Width of the EUC (km). (c) Mean seasonal cycle of the depth at $\sigma_\theta$ = 25.5 isopycnal depth from the PIRATA buoy at 10°W compared to the cruise data (circles). The dashed curves represent the standard deviation of the annual cycle from the PIRATA buoy. The squares indicate the depth of the maximum velocity core. (d) Mean seasonal cycle of the thermocline thickness between $\sigma_\theta$ = 24.5–26.5 isopycnal surfaces from PIRATA buoy at 10°W compared to the cruise data (stars).

corresponds to the late fall intensification of the SEC within the equatorial band [*Richardson and McKee*, 1984]. In the deep thermocline, this indicates that the deepest part of the eastward flow is a transient feature of the equatorial circulation, unlike the EUC located within the upper and lower thermocline that is quasi-permanent all along the year. Besides, the isopycnal $\sigma_\theta$ = 24.5 no longer outcrops and the EUC core lies again along the $\sigma_\theta$ = 25.5 isopycnal.

### 4.3. Variability in EUC Core and Thermocline Properties

[35] As seen before, an important ingredient for the seasonal variability of the EUC transport is the vertical extension of the EUC that flows in the deep thermocline in boreal summer. However, two other variables may modulate the EUC transport: the eastward velocity amplitude and the EUC width. Eastward velocity maximum values measured in the EUC are provided in Table 3 and reported in Figure 5a. The eastward velocity maximum ranges from 57 cm s$^{-1}$ to 108 cm s$^{-1}$, but does neither exhibit a well marked variability along the year, nor a significant correlation with the EUC transport seasonal variability. Thus, we cannot identify any obvious link between the EUC maximum velocity and the EUC semiannual cycle from our velocity data sets.

[36] The width of the EUC core, presented in Figure 5b and Table 3, suggests a strong variability (from 178 km in June 2007 to 522 km in March 2000) at 10°W during the year. As in the work by *Arhan et al.* [2006], the measurements of the EUC width at 10°W suggest two maxima: a first one in March (up to 520 km) and a second one from September to November (greater than 370 km), indicating a probable semiannual cycle for the EUC width. Nevertheless this semiannual cycle does not coincide with that of the EUC transport. In particular the EUC width is found to be minimum in boreal summer when the EUC transport is the strongest of the year. It is maximum in boreal fall. The situation in boreal spring (when the EUC width is maximum while its transport is minimum) and winter is more complex since we do not have enough data in these seasons to provide any robust conclusion.

[37] In conclusion, the seasonal EUC transport cannot be explained by the EUC width or the velocity maximum at the core of the EUC. So the main parameter controlling the

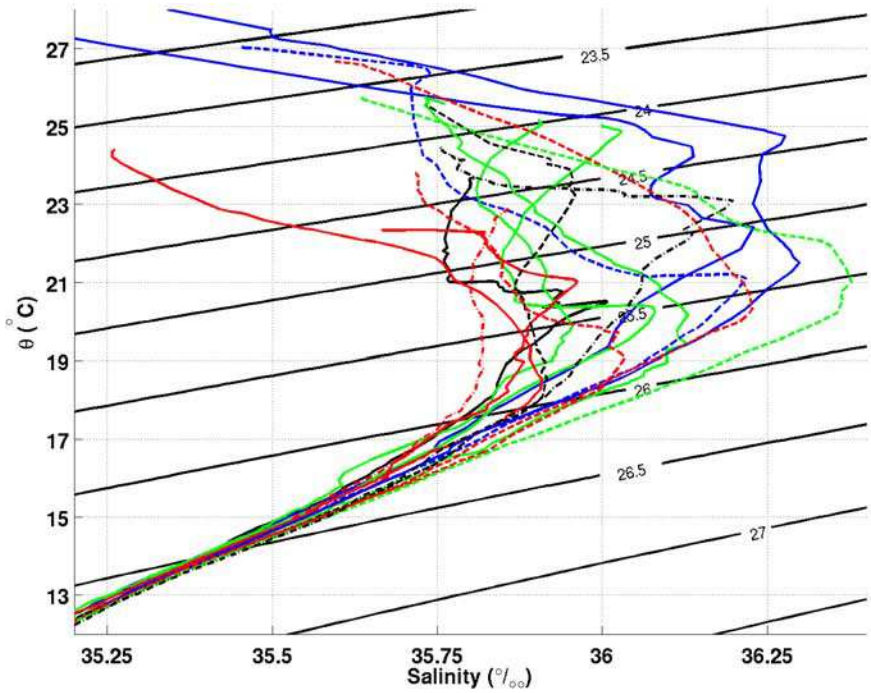


**Figure 6.** The $\theta$-$S$ diagram at 0°N–10°W from 15 cruises. The red profiles correspond to the summer (June 2005, dash-dotted; June 2006 and June 2007, dashed; August 1999 and August 2000, solid); the black profiles correspond to September (September 1997, solid; September 2005, dashed; September 2007, dash-dotted); the green profiles correspond to the fall (October 1999, October 2001, and November 2000, solid; November 2006, dashed); and the blue profiles correspond to the winter (December 2002, dashed; January 1999 and February 2004, solid).

seasonal cycle must be the deep extension of the EUC into the lower and deep thermocline.

[38] Now we focus on the variability of the thermocline depth (defined as the depth of the $\sigma_\theta$ = 25.5 isopycnal) and thermocline thickness (defined as the thickness between the $\sigma_\theta$ = 24.5 and 26.5 isopycnals), that are summarized in Table 3. These values are reported in Figures 5c and 5d, along with their mean seasonal cycles estimated from the temperature data provided by the PIRATA buoy at 10°W–0°N.

[39] Both cruises and PIRATA data sets indicate a semi-annual cycle for the thermocline depth and thickness that are well correlated with the EUC transport one. The thermocline depth (squares) presents minimum values in June–August (shallower than 50 m depth) and a second minimum between mid-November and January (shallower than 65 m). It is maximum during boreal spring (around 70 m) and September–October (deeper than 70 m).

[40] The thermocline thickness presents the strongest maximum from June to September (around 175 m), with a weaker maximum in December–January (up to 155 m), and is minimum in February–March and in October–November (around 140 m). The thermocline depth and thickness vary seasonally in phase, but the summer maximum of the thermocline thickness lasts about three months, and remains almost constant in August–September whereas the thermocline deepens.

[41] As summarized in Table 3 and Figure 5c, the depth of the EUC velocity core (circles) presents a seasonal variability with minimum values in winter and summer (around 60 m) and maximum values from September to December (around 80 m). Moreover, the comparison with the thermocline depth (squares) shows that the EUC core is clearly located under the thermocline ($\sigma_\theta$ = 25.5 isopycnal) in summer, and in lesser extent in November–December, and about at the level of the $\sigma_\theta$ = 25.5 during the rest of the year. The moderate amplitude of the seasonal vertical migration of the EUC core (20 m) indicates that the depth of the EUC core varies weakly in depth in comparison with the large vertical movements of the thermocline (50 m). Thus, the $\sigma_\theta$ = 25.5 isopycnal is not bound to the EUC core, but moves above the EUC core during upwelling seasons.

### 4.4. Variability of EUC Water Masses

[42] The upward and downward movements of the thermocline also explain the observed seasonal variations of the salinity core associated with the EUC, as illustrated in Figure 6 that presents the temperature-salinity profiles observed at 0°N–10°W during each cruise. During all cruises, the salinity maximum is observed between the $\sigma_\theta$ = 24.5 and 25.5 isopycnals.

[43] During the boreal winter cruises (blue profiles), the salinity core is well developed and exceeds 36.2. The salinity section in January 1999 (Figure 7a) shows a large salinity core associated with the EUC velocity core (Figure 5a) reaching a concentration as high as 36.4 in the upper thermocline at the equator. The salinity maximum is strongly eroded during the boreal summer cruises (red profiles), decreasing down to 35.9. It is noticeable that in June 2005 (Figure 7b) the salinity core associated with the

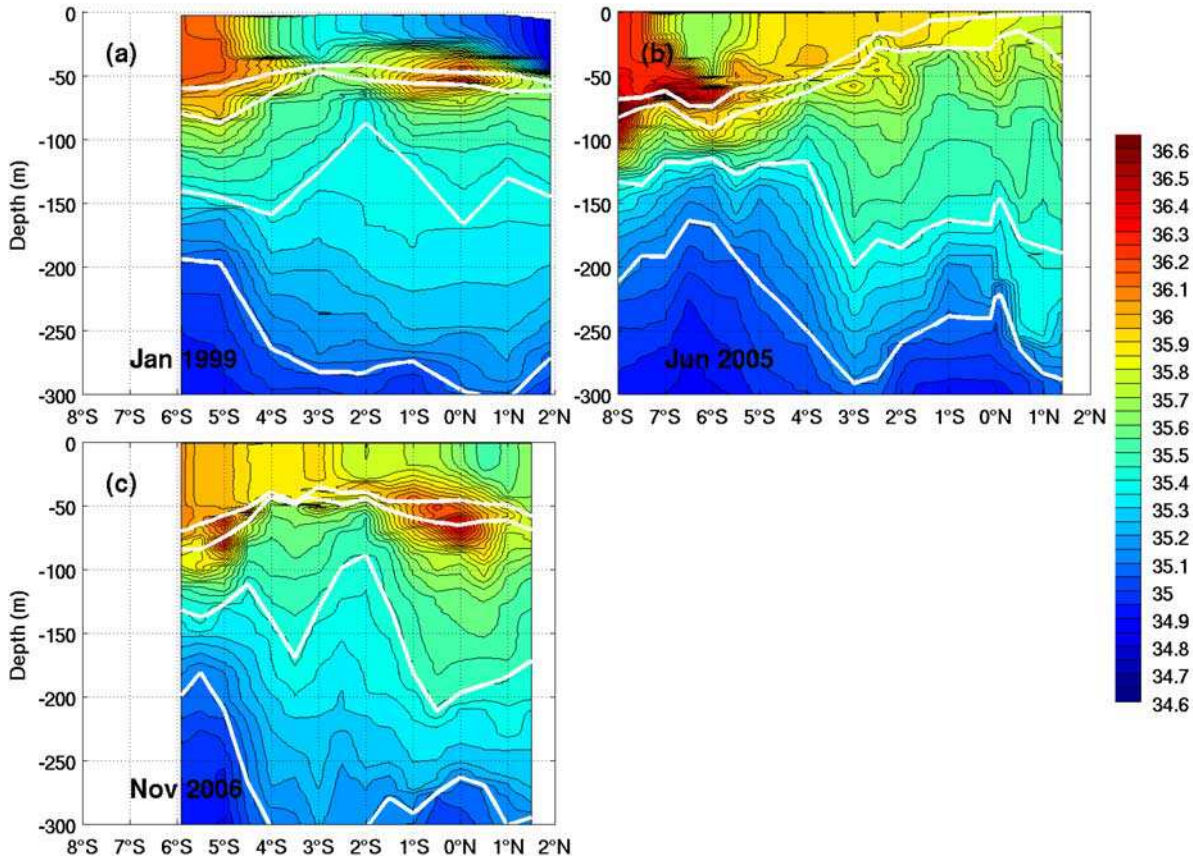


**Figure 7.** Meridional sections of salinity at 10°W between 300 m depth and the surface and 8°S and 2°N (a) during PIRATA-FR3 cruise in January 1999, (b) during EGEE 1 cruise in June 2005, and (c) during EGEE 4 cruise in November 2006.

EUC is totally eroded (dashed dotted red curve), while in June 2007 and in a lesser extent in June 2006, the EUC salinity core is still well developed, like in boreal winter (dashed red curves). This suggests an important interannual variability at the beginning of the equatorial upwelling season. This feature is concomitant to the outcropping of the upper thermocline into the mixed layer (Figure 7b [*Gouriou and Reverdin*, 1992]). Thus, during this period of the year, the eastward velocity core no longer presents a salinity maximum, and no longer advects eastward the saline subtropical water masses that characterize the mean EUC (Figures 2a and 2b).

[44] From September to November (black and green profiles), the salinity maximum is observed again above $\sigma_\theta$ = 25.5, implying that the western ventilation of subtropical waters is active again, as illustrated in Figure 4c for November 2006. The profiles in September 2005 and 2007 (black dashed curves) show that the salinity maximum is well reformed in the upper thermocline (along $\sigma_\theta$ = 24.5), with a weaker secondary maximum along the isopycnal $\sigma_\theta$ = 26.0 in September 2005, producing an obvious double core vertical structure. This double core is probably due to the reappearance of eastward advection of surface saline water from the west at the end of the upwelling season. Note that this double core is also present in all boreal winter profiles (blue curves).

[45] The vertical distribution of salinity at the equator thus experiences a strong seasonal cycle, whose most striking manifestation is the strong erosion of the salinity maximum associated with the EUC during the boreal summer upwelling. Such an erosion may also occur in boreal winter as evidenced in December 2002 during the second upwelling season [*Okumura and Xie*, 2006], though with a weaker amplitude and located in the shallowest upper thermocline (above $\sigma_\theta$ = 25.0).

### 4.5. Variability of the SEUC

[46] The main characteristics and transport estimates of the SEUC are provided in Table 4 and in Figure 8. The SEUC transport varies between 1.5 Sv (minimum value in March 2000) and 11.6 Sv (maximum value in November 2006), but it must be remembered that the cutoff depth of the SADCP generally does not allow to observe the full vertical extent of the SEUC, thus underestimating its zonal transport. The range of maximum zonal velocity is between 20 cm s$^{-1}$ (in March 2000) and 55 cm s$^{-1}$ (in August 2004). This leads to a mean maximum of 39 cm s$^{-1}$ which is far greater than the maximum velocity (15 cm s$^{-1}$) deduced from the mean section (Figure 2a). Both parameters (transport and velocity) do not exhibit any clear seasonal cycle (Figures 8a and 8b).

[47] Both the latitudinal position and depth of the maximum velocity of the SEUC vary significantly according to the cruise data. There are some indication that it is more poleward (beyond 5°S) and deeper (beneath 140 m) between February and July, and closer to the equator

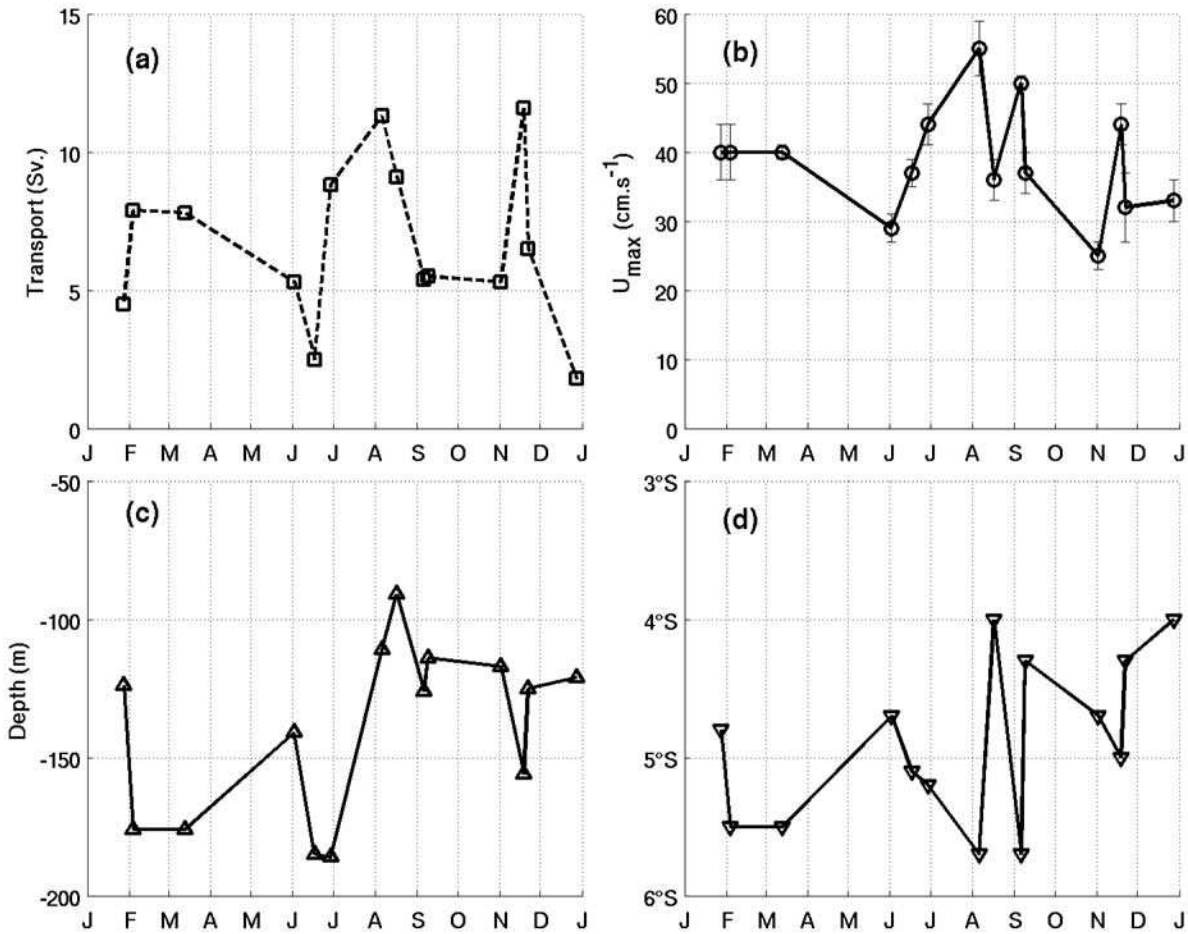


**Figure 8.** Repartition during the year of the main SEUC parameters at 10°W: (a) eastward transport (Sv), (b) maximum zonal velocity (m s$^{-1}$), (c) depth of SEUC core (m), and (d) latitude of the SEUC core (in degrees).

(northward of 5°S) and above 130 m depth during both boreal fall cruises (Figure 8c), but no clear seasonal cycle can be unambiguously evidenced. In particular, large variations of the latitudinal position and depth of the SEUC are observed during the three cruises carried out in August, when the SEUC depth varies from 91 m in 2000 up to 178 m in 1999, and when the SEUC latitude ranges from 4°S in 2000 to 5.5°S in 1999 along 10°W. This suggests an important intraseasonal or interannual variability in the SEUC properties, especially in boreal summer.

[48] In August 2004 (not shown) the eastward flow associated with the SEUC extends up to the surface at 6°W, indicating the possibility of a surfacing of the SEUC in the GG. Such a SEUC surfacing has already been observed at 3°E in boreal winter 1995 [*Mercier et al.*, 2003].

## 5. Discussion

[49] The seasonal cycle of the EUC transport has been shown to strongly depend upon the zonal circulation in the lower and deep thermocline at 10°W, the boreal summer maximum being in large part explained by the presence of intense eastward flow beneath 150 m as observed during all summer cruises. Figure 9 presents the time-depth distribution of zonal velocity between May 2003 and July 2005

**Table 4.** Main Characteristics Observed for the SEUC During Each Cruise[a]

| | Longitude | Vmax (cm s$^{-1}$) | Z (m) | Latitude (deg) | Transport (Sv) |
|---|---|---|---|---|---|
| Date | | | | | |
| Jan 1999 | 10°W | 40 ± 4 | 124 | −4.8 | 4.5 |
| Feb 2004 | 10°W | 40 ± 4 | 176 | −5.5 | 7.9 |
| Mar 2000 | 10°W | 20 ± 1 | 158 | −4.2 | 1.5 |
| May 2003 | 6°W | 30 ± 3 | 142 | −4.5 | 2.7 |
| Jun 2005 | 10°W | 37 ± 2 | 185 | −5.1 | 5.8 |
| Jun 2006 | 10°W | 29 ± 2 | 141 | −4.7 | 5.3 |
| Jun 2007 | 10°W | 44 ± 3 | 186 | −5.2 | 8.8 |
| Aug 1999 | 10°W | 23±4 | 178 | −5.5 | 3.6 |
| Aug 2000 | 10°W | 36 ± 3 | 91 | −4 | 9.1 |
| Aug 2004 | 6°W | 55 ± 4 | 111 | −5.7 | 11.3 |
| Sep 2005 | 10°W | 50 ± 1 | 126 | −5.7 | 5.4 |
| Sep 1997 | 10°W | 37 ± 3 | 114 | −4.3 | 5.5 |
| Oct 2001 | 10°W | 25 ± 2 | 107 | −4.7 | 5.3 |
| Nov 2006 | 10°W | 44 ± 3 | 156 | −5 | 11.6 |
| Nov 2000 | 10°W | 32 ± 5 | 125 | −4.3 | 6.5 |
| Dec 2002 | 10°W | 33 ± 3 | 121 | −4 | 1.8 |
| Means | 10°W | 39 ± 9 | 139 ± 31 | −4.9 ± 0.6 | 6.7 ± 2.9 |
| Averaged section | 10°W | 15 ± 5 | 125 | −5.1 | 4.3 |

[a]First column, month of the campaign along with means and averaged section; second column, longitude of the section; third column, maximum velocity of the SEUC; fourth column, depth of the SEUC core; fifth column, latitude of the SEUC; and sixth column, estimated transport of the SEUC (the estimated transports of the SEUC are underestimated because of the SADCP cutoff).

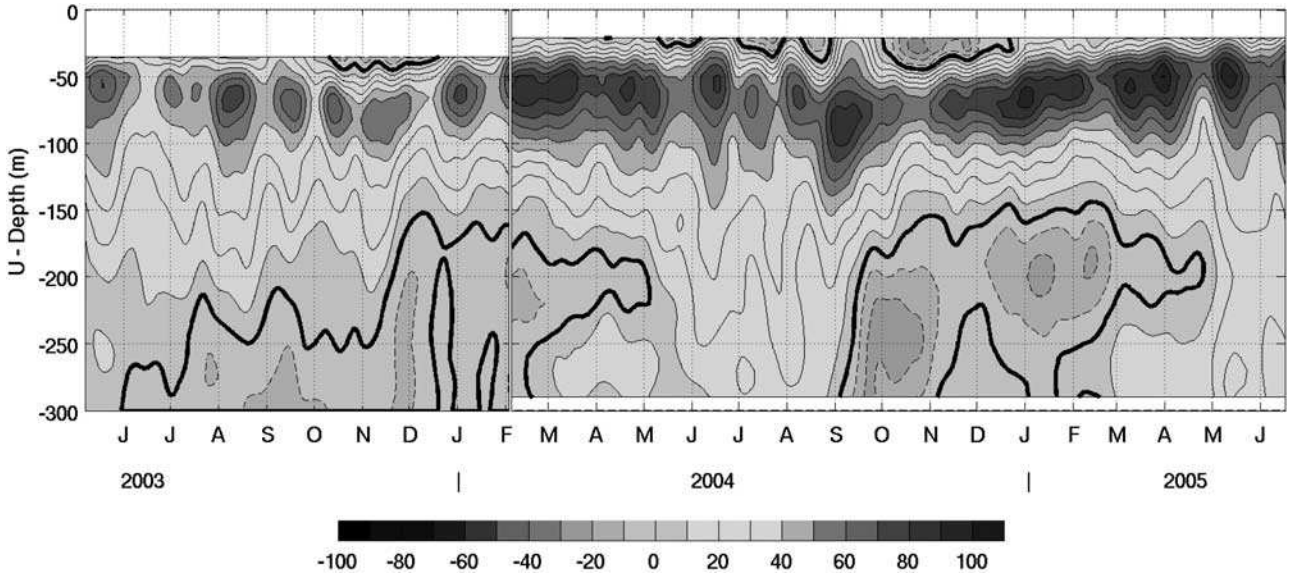


**Figure 9.** Zonal velocity (cm $s^{-1}$) from mooring at 0°N–10°W during 2003–2005 between 0 and 300 m depth. Bold curves refer to the isotach 0, and dashed curves refer to negative velocities.

above 300 m from the PIRATA ADCP mooring at 10°W–0°N. The more remarkable variability in zonal velocity is found between 150 m and 250 m, with eastward currents observed each year between May and September and westward currents the remaining of the year. This is consistent with the annual reversal of zonal currents that was previously described from our sparse SADCP measurements. This reversal thus appears as a recurrent feature of the zonal circulation in subsurface at 10°W. The comparison of boreal summer eastward currents from 2003 to 2005 shows significant interannual variability at 200 m with stronger currents in 2004 and 2005 (exceeding 20 cm $s^{-1}$), and weaker ones in 2003.

[50] Note that below 250 m, a reversal of zonal currents is also observed, but eastward velocities appears earlier (in February–March) than at 200 m (in May), both in 2004 and 2005. From March to May, these deep eastward velocities are separated from the EUC by a thin layer of westward velocity around 200 m depth, so that the eastward transport associated with this deep current is not included in the EUC transport. This feature has been previously reported by *Verstraete* [1992]. Conversely from March to September 2004, eastward velocities below 250 m are connected to the EUC because of the presence of the deep extension down to 300 m.

[51] To determine the role of the zonal pressure gradient (ZPG) for the dynamics of the EUC at 10°W, Figure 10a presents the mean seasonal evolution of the acceleration term due to ZPG. Around 50 m depth, the ZPG is always positive with a predominant semiannual cycle. The acceleration due to ZPG above 100 m depth is the strongest from May to September and from December to February, and the weakest (almost vanishing or even negative near the surface) in March and November. Even though semiannual variability is evidenced in both ZPG and the upper EUC transport (Figure 3c), no clear phase lag can be deduced.

[52] Below 100 m, the variability is mainly annual, the acceleration term due to the ZPG being positive from February to August and negative from August to December. The strong maximum observed in April and the strong minimum observed in September–October are compatible with the appearance of eastward velocities in the deep thermocline from April–May and their disappearance from September. These observations suggest that the ZPG and the velocities are in quadrature below 100 m, which is compatible with the linear theory of equatorial waves. These results indicate that the ZPG is likely to play an important role for the dynamics of the EUC seasonal evolution at 10°W.

[53] Figure 10b presents the seasonal anomalies of the zonal wind at the location of the PIRATA moorings. The annual mean of the wind has been removed. At 10°W (solid black curve), the seasonal cycle of the wind is predominantly semiannual with a weakening of the Easterlies in February–March and September–October, and a reinforcement of Easterlies from May to July, and to a lesser extent in November–December. This semiannual evolution of the wind at 10°W–0°N is in good agreement with the seasonal cycle of the near-surface ZPG described above. The comparison of PIRATA winds at 10°W and at other longitudes (Figure 10b) shows that the semiannual cycle is dominant in the GG (10°W and 0°E), whereas the annual cycle dominates the variability at 35°W. At 23°W both annual and semiannual cycles are present. These results indicate that a semiannual cycle of the EUC and of the ZPG in the upper 100 m are compatible with the local zonal wind forcing east of 23°W.

[54] Our data set suggests that the eastward flow at 10°W must be divided in two parts. In the lower and upper thermocline, the EUC is permanent all along the year. Both EUC transports in these isopycnal ranges and the thermocline depth experience a predominant semiannual cycle that is compatible with the ZPG and local zonal winds. These results are consistent with the numerical studies of *Philander and Pacanowski* [1986] and *Giarolla et al.* [2005]. However, *Philander and Pacanowski* [1986]

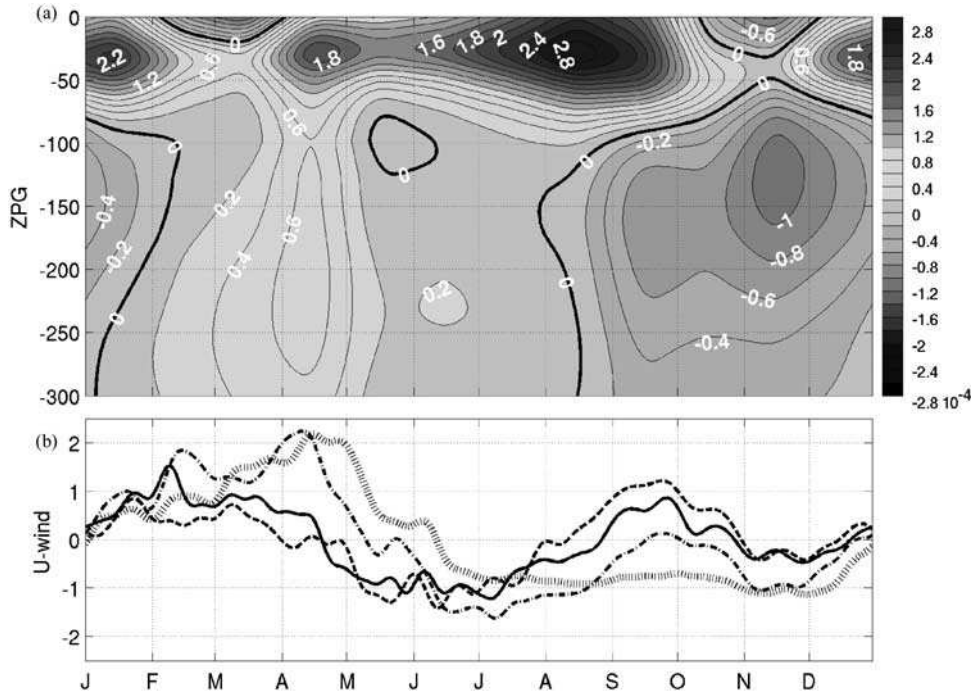


**Figure 10.** (a) Mean annual cycle of the zonal pressure gradient (ZPG) ($N^2$ $m^{-3}$) with respect to depth at 0°N–23°W, 0°N–10°W, and 0°N–0°E calculated from the ARIVO climatology with a reference level at 500 m depth. (b) Seasonal anomalies of zonal wind speeds (m $s^{-1}$) at 4 m from PIRATA mooring at 0°N–35°W (hatched), 0°N–23°W (dash-dotted), 0°N–10°W (solid), and 0°N–0°E (dashed) for the period 1997–2007.

and *Weisberg and Tang* [1990] have also shown that part of the semiannual cycle in the upper layers of the equatorial Atlantic could also result from the basin wide adjustment to the sudden reinforcement of the Easterlies in the central and eastern parts of the basin between March and June.

[55] Our results also suggest that the EUC at 10°W is rather located under the thermocline, contrarily to the western EUC always found within the thermocline [*Schott et al.*, 2003; *Brandt et al.*, 2006]. Our results show a strong semiannual variability of the EUC transport and indicate that the hydrological structure varies strongly above and beneath the EUC velocity core. The depth of the EUC core does not vary significantly and is always located within 50 and 70 m depth. It is deeper in fall and winter, and shallower in late spring and summer. The hydrological structure moves seasonally upward and downward, and strongly outcrops during late spring and summer [*Voituriez*, 1983; *Verstraete*, 1992]. Consequently, the thermocline moves under or above the EUC velocity core, not only leading to significant variations in the vertical distribution of the EUC transport according to isopycnal layers, but also to the strong seasonal erosion of the upper EUC high-salinity core within the mixed layer. One strong characteristic of the EUC at 10°W is thus that it does not transport eastward the saline subtropical water masses all along the year, in contrast with more western longitudes where the salinity maximum is permanently associated with the EUC core.

[56] Unlike the upper and lower thermocline, the deep branch of the eastward flow (below the EUC in the deep thermocline) is not permanent, but transient. Eastward velocities are present only in boreal summer providing an important contribution (between 5 Sv and 15 Sv) to the total eastward transport across 10°W during boreal summer. *Philander and Pacanowski* [1987] suggest that the annual reversal of the zonal currents in the deep thermocline could be nonlinearly forced by the vertical movement of the thermocline, that heaves up and down with large amplitude in the eastern Atlantic. Such a mechanism is also evidenced by *Thierry et al.* [2004] from numerical simulations, in which a large number of high vertical modes are excited in the same region. This annual variability could also be linked to the downward traveling of Rossby wave of the gravest meridional mode emanating from the eastern Atlantic [*Thierry et al.*, 2004; *Brandt and Eden*, 2005], as suggested farther west, around 23°W, by *Brandt et al.* [2006], who observe a similar reversal of zonal currents between 240 and 400 m depth associated with upward phase propagations. This feature has been also evidenced earlier from in situ observations in the Pacific ocean by *Lukas and Firing* [1985]. Low-frequency (annual) Rossby waves could be generated in the east by both local wind or/and the reflection of annual Kelvin waves against the eastern boundary [*McCreary et al.*, 1984].

[57] The composite seasonal cycle of the transport may also be altered by some interannual anomalies, like "Atlantic El Niño" [*Zebiak*, 1993]. *Marin et al.* [2009] have shown, for instance, that June conditions in 2005 and 2006 were extreme, with strong anomalous cold conditions in 2005 and strong anomalous warm conditions in 2006. Such interannual anomalies may be responsible for important changes in the subsurface conditions along the equator

during the period of observation (1997–2007), for instance the weaker EUC transport in June 2005 than in June 2006 [e.g., *Hormann and Brandt*, 2009]. Our limited in situ observations do not allow to quantify precisely how they alter the composite seasonal cycle of the EUC transport that is described in the paper. However, the agreement between cruises data, PIRATA mooring temperature measurements and ZPG estimated from the ARIVO climatology tend to suggest the robustness of the composite seasonal cycle we have evidenced.

## 6. Conclusion

[58] We presented in this study an original new set of 17 SADCP sections along 10°W, including 15 with hydrological measurements, carried out between 1997 and 2007. The EUC presents at 10°W an averaged transport of 12.1 ± 1.9 Sv, but the average of the eastward transports estimated from the 17 individual sections is found to be 15.9 ± 7.6 Sv, which is the signature of a large variability of the eastward transport, in particular in the deep layer below $\sigma_\theta = 26.5$. These two estimates encompass the EUC transport of 13.8 Sv found by *Brandt et al.* [2006] around 23°W. The transport of the mean EUC from mean section, that is directly comparable to those of *Brandt et al.* [2006] at 23°W, indicate a modest weakening of the EUC transport between 23°W and 10°W for the permanent EUC in the upper thermocline. In addition to this permanent current, transient eastward velocities are observed below $\sigma_\theta = 26.5$ and strongly intensify the eastward transport near the equator in boreal summer. However, the mean annual transport in the deep thermocline layer is only 0.9 Sv, indicating that it contributes only weakly to the mean eastward advection of thermocline water masses. The average of EUC transports (15.9 Sv), taking only into account eastward velocities, is likely to overestimate the contribution of the eastward currents in the deep thermocline for the EUC transport.

[59] Our observations suggest the existence of a seasonal cycle for the EUC transport, with a dominant annual harmonics and some indications of a somewhat weaker semiannual cycle, but the under sampling during boreal spring and possible intraseasonal/interannual variability in the subsurface conditions may moderate this conclusion. However, the two EUC transport maxima that are systematically observed in January–February and, with a stronger magnitude, between June and September are consistent with results based on numerical studies [*Philander and Pacanowski*, 1986; *Arhan et al.*, 2006]. At 10°W, the EUC transport maximum measured in summer is also associated with a strong intensification of the eastward transport in the deep thermocline. This deep extension is present only in boreal summer and reverses into a westward current in boreal fall, suggesting the transient character of the deep flow just below the EUC in contrast to the permanent EUC core. Such an annual deep extension of eastward velocity is not observed west of 10°W, even though annual transient currents are also observed below the EUC at the EIC depth at 23°W [*Brandt et al.*, 2006] and in middepth (around 800 and 1500 m depth) at 35°W [*Brandt and Eden*, 2005]. More investigation is needed to understand the mechanisms that control the annual cycle in the equatorial Atlantic.

[60] An important aspect of the variability of the EUC core at 10°W is the disappearance of the salinity maximum, that characterizes the EUC at 35°W and 23°W in boreal summer [*Schott et al.*, 2003; *Brandt et al.*, 2006]. It is related to the boreal summer outcropping of the upper hydrological structure, associated with equatorial upwelling. One important consequence is that the subtropical waters of the ventilated thermocline [*Reverdin et al.*, 1993] must outcrop in the surface mixed layer west of 10°W, and no longer penetrate into the GG in boreal summer.

[61] The in situ data used in this study, that are principally from recent cruises and moorings of the PIRATA program, allowed us to better understand the seasonal variability of the equatorial circulation at the entrance of the GG. Such an analysis has to be continued, for instance through numerical studies, in order to precisely identify and understand all dynamical processes responsible for this variability. In this way, this analysis has to be seen as a first step for our understanding of upper layer processes in the eastern equatorial Atlantic. Such processes are crucial for the properties of the cold tongue and of the equatorial and coastal upwellings, and for the variability of the regional climate. It is one of the main goals of the AMMA, PIRATA and CLIVAR/TACE (see http://www.clivar.org/organization/atlantic/TACE/tace.php) programs to study these near-surface oceanic processes.

[62] **Acknowledgments.** On the basis of a French initiative, AMMA was built by an international scientific group and is currently funded by a large number of agencies, especially from France, the United Kingdom, the United States, and Africa. It has been the beneficiary of a major financial contribution from the European Community's Sixth Framework Research Programme. Detailed information on scientific coordination and funding is available on the AMMA International Web site, http://www.amma-international.org. The authors thank Fabienne Gaillard and Karina von Schuckmann for kindly providing ARIVO climatology data. The authors also thank the PIRATA program for providing precious data sets for free to the whole scientific community and all the technicians and vessels' crews who made possible the in situ data acquisition. We thank Yves Gouriou, Herlé Mercier, and Jérôme Sirven for constructive discussions during this work and the two anonymous reviewers for constructive remarks on the paper.

## References

Arhan, M., A. Treguier, B. Bourlès, and S. Michel (2006), Diagnosing the annual cycle of the Equatorial Undercurrent in the Atlantic Ocean from a general circulation model, *J. Phys. Oceanogr.*, *36*, 1502–1522.

Bourlès, B., Y. Gouriou, and R. Chuchla (1999), On the circulation in the upper layer of the western equatorial Atlantic, *J. Geophys. Res.*, *104*, 21,151–21,170.

Bourlès, B., M. D'Orgeville, G. Eldin, Y. Gouriou, R. Chuchla, Y. DuPenhoat, and S. Arnault (2002), On the evolution of the thermocline and subthermocline eastward currents in the equatorial Atlantic, *Geophys. Res. Lett.*, *29*(16), 1785, doi:10.1029/2002GL015098.

Bourlès, B., et al. (2008), The PIRATA program: History, accomplishments, and future directions, *Bull. Am. Meteorol. Soc.*, *89*, 1111–1125.

Brandt, P., and C. Eden (2005), Annual cycle and interannual variability of the mid-depth tropical Atlantic Ocean, *Deep Sea Res., Part I*, *52*, 199–219.

Brandt, P., F. A. Schott, C. Provost, A. Kartavtseff, V. Hormann, B. Bourlès, and J. Fischer (2006), Circulation in the central equatorial Atlantic: Mean and intraseasonal to seasonal variability, *Geophys. Res. Lett.*, *33*, L07609, doi:10.1029/2005GL025498.

Bunge, L., C. Provost, and A. Kartavtseff (2007), Variability in horizontal current velocities in the central and eastern equatorial Atlantic in 2002, *J. Geophys. Res.*, *112*, C02014, doi:10.1029/2006JC003704.

Dessier, A., and J. R. Donguy (1994), The sea surface salinity in the tropical Atlantic between 10°S and 30°N—Seasonal and interannual variations (1977–1989), *Deep Sea Res., Part I*, *41*, 81–100.

Fofonoff, P., and R. Millard (1983), Algorithms for computation of fundamental properties of seawater, *UNESCO Tech. Pap. Mar. Sci.*, *44*, 53 pp.
Gaillard, F., E. Autret, V. Thierry, P. Galaup, C. Coatanoan, and T. Loubrieu (2009), Quality control of large Argo data sets, *J. Atmos. Oceanic Technol.*, *26*, 337–351.
Giarolla, E., P. Nobre, M. Malagutti, and L. P. Pezzi (2005), The Atlantic Equatorial Undercurrent: PIRATA observations and simulations with GFDL Modular Ocean Model at CPTEC, *Geophys. Res. Lett.*, *32*, L10617, doi:10.1029/2004GL022206.
Gouriou, Y., and G. Reverdin (1992), Isopycnal and diapycnal circulation of the upper equatorial Atlantic Ocean in 1983–1984, *J. Geophys. Res.*, *97*, 3543–3572.
Hazeleger, W., P. de Vries, and Y. Friocourt (2003), Sources of the Equatorial Undercurrent in the Atlantic in a high resolution ocean model, *J. Phys. Oceanogr.*, *33*, 677–693.
Hisard, P., and C. Hénin (1987), Response of the equatorial Atlantic Ocean to the 1983–1984 wind from the Programme Français Océan et Climat dans l'Atlantique equatorial cruise data set, *J. Geophys. Res.*, *92*, 3759–3768.
Hormann, V., and P. Brandt (2009), Upper equatorial Atlantic variability during 2002 and 2005 associated with equatorial Kelvin waves, *J. Geophys. Res.*, *114*, C03007, doi:10.1029/2008JC005101.
Katz, E., R. Molinari, D. Cartwright, P. Hisard, H. Lass, and A. deMesquita (1981), The seasonal transport of the Equatorial Undercurrent in the western Atlantic (during the Global Weather Experiment), *Oceanol. Acta*, *4*, 445–450.
Lukas, R., and E. Firing (1985), The annual Rossby wave in the central equatorial Pacific Ocean, *J. Phys. Oceanogr.*, *15*, 55–67.
Lux, M., H. Mercier, and M. Arhan (2001), Interhemispheric exchanges of mass and heat in the Atlantic Ocean in January–March 1993, *Deep Sea Res., Part I*, *48*, 605–638.
Marin, F., G. Caniaux, B. Bourlès, H. Giordani, Y. Gouriou, and E. Key (2009), Why were sea surface temperatures so different in the eastern equatorial Atlantic in June 2005 and 2006?, *J. Phys. Oceanogr.*, in press.
McCreary, J., J. Picaut, and D. Moore (1984), Effects of remote annual forcing in the eastern tropical Atlantic Ocean, *J. Mar. Res.*, *42*, 45–81.
Mercier, H., M. Arhan, and J. Lutjeharms (2003), Upper-layer circulation in the equatorial and South Atlantic Ocean in January–March 1995, *Deep Sea Res., Part I*, *50*, 863–887.
Millero, F. J., C.-T. Chen, A. Bradshaw, and K. Schleicher (1980), A new high pressure equation of state for seawater, *Deep Sea Res., Part A*, *27*, 255–264.
Okumura, Y., and S.-P. Xie (2006), Some overlooked features of tropical Atlantic climate leading to a new Niño-like phenomenon, *J. Clim.*, *19*, 5859–5874.
Philander, S., and R. Pacanowski (1986), A model of the seasonal cycle of the tropical Atlantic Ocean, *J. Geophys. Res.*, *91*, 14,192–14,206.
Philander, S., and R. Pacanowski (1987), Nonlinear effects in the seasonal cycle of the tropical Atlantic Ocean, *Deep Sea Res., Part A*, *34*, 123–137.
Redelsperger, J.-L., C. D. Thorncroft, A. Diedhiou, T. Lebel, D. J. Parker, and J. Polcher (2006), African monsoon multidisciplinary analysis: An international research project and field campaign, *Bull. Am. Meteorol. Soc.*, *87*, 1739–1746.
Reverdin, G., R. Weiss, and W. Jenkins (1993), Ventilation of the Atlantic Ocean equatorial thermocline, *J. Geophys. Res.*, *98*, 16,289–16,310.
Richardson, P., and T. McKee (1984), Average seasonal variation of the Atlantic equatorial current from ship drift data, *J. Phys. Oceanogr.*, *14*, 1226–1238.
Schott, F. A., J. Fischer, and L. Stramma (1998), Transports and pathways of the upper-layer circulation in the western tropical Atlantic, *J. Phys. Oceanogr.*, *28*, 1904–1928.
Schott, F. A., M. Dengler, P. Brandt, K. Affler, J. Fischer, B. Bourlès, Y. Gouriou, R. L. Molinari, and M. Rhein (2003), The zonal currents and transports at 35°W in the tropical Atlantic, *Geophys. Res. Lett.*, *30*(7), 1349, doi:10.1029/2002GL016849.
Servain, J., A. J. Busalacchi, M. J. McPhaden, A. D. Moura, G. Reverdin, M. Vianna, and S. E. Zebiak (1998), A Pilot Research Moored Array in the Tropical Atlantic (PIRATA), *Bull. Am. Meteorol. Soc.*, *79*, 2019–2031.
Stramma, L., and F. Schott (1999), The mean flow field of the tropical Atlantic Ocean, *Deep Sea Res., Part II*, *46*(1–2), 279–303.
Thierry, V., A.-M. Treguier, and H. Mercier (2004), Numerical study of the annual and semi-annual fluctuations in the deep equatorial Atlantic Ocean, *Ocean Modell.*, *6*, 1–30.
Tsuchiya, M. (1986), Thermostads and circulation in the upper layer of the Atlantic Ocean, *Prog. Oceanogr.*, *16*, 235–267.
Verstraete, J.-M. (1992), The seasonal upwellings in the Gulf of Guinea, *Prog. Oceanogr.*, *29*, 1–60.
Voituriez, B. (1983), Les variations saisonnières des courants équatoriaux à 4°W et l'upwelling équatorial du Golfe de Guinée, I. Le sous-courant équatorial, *Oceanogr. Trop.*, *18*(2), 163–183.
Wacongne, S., and B. Piton (1992), The near-surface circulation in the northeastern corner of the South Atlantic Ocean, *Deep Sea Res., Part A*, *39*, 1273–1298.
Weisberg, R., and T. Tang (1990), A linear analysis of equatorial Atlantic Ocean thermocline variability, *J. Phys. Oceanogr.*, *20*, 1813–1825.
Zebiak, S. E. (1993), Air-sea interaction in the equatorial Atlantic region, *J. Clim.*, *6*, 1567–1586.
Zhang, D., M. McPhaden, and W. Johns (2003), Observational evidence for flow between the subtropical and tropical Atlantic: The Atlantic subtropical cells, *J. Phys. Oceanogr.*, *33*, 1783–1797.

B. Bourlès, LEGOS, IRD, CRHOB, Résidence les Cocotiers, 08 B.P. 841, Cotonou, Benin.
R. Chuchla and F. Marin, LEGOS, IRD, F-31400 Toulouse, France.
J. Grelet, US191, IRD, F-29280 Plouzané, France.
N. Kolodziejczyk, LEGOS, IRD, Technopole Pointe du Diable, B.P. 70, F-29280 Plouzané, France. (nicolas.kolodziejczyk@gmail.com)